Investigation of a chaotic thermostat

G. J. Morales

Phys. Rev. E **97**, 032203 — Published 8 March 2018

DOI: 10.1103/PhysRevE.97.032203

Investigation of a chaotic thermostat

G. J. Morales

Department of Physics and Astronomy,

University of California, Los Angeles, California 90025

Abstract

A numerical study is presented of a free particle interacting with a deterministic thermostat in which the usual friction force is supplemented with a fluctuating force that depends on the self-consistent damping coefficient associated with coupling to the heat bath. It is found that this addition results in a chaotic environment in which a particle self-heats from rest and moves in positive and negative directions, exhibiting a characteristic diffusive behavior. The frequency power spectrum of the dynamical quantities displays the exponential frequency dependence ubiquitous to chaotic dynamics. The velocity distribution function approximates a Maxwellian distribution, but it does show departures from perfect thermal equilibrium, while the distribution function for the damping coefficient shows a closer fit. The behavior for the classic Nosé-Hoover (NH) thermostat is compared to that of the enlarged Martyna-Klein-Tuckerman (MKT) model. Over a narrow amplitude range, the application of a constant external force results quantitatively in the Einstein relation for the NH thermostat, and for the MKT model it differs by a factor of 2.

PACS: 05.45 Ac, 0.545 Jc, 05.45 Pq, 05.70 Ln

I. INTRODUCTION

The study of deterministic thermostats [1-4] has resulted in extensive investigations [5-9] of physical systems and, perhaps more importantly, it has provided insight about the connection of statistical mechanics to nonlinear dynamics, particularly the recognition of the subtle role played by chaotic orbits [10]. Because of its simplicity and transparent physical interpretation, the paradigm system of this subject is the Nosé-Hoover (NH) model [11]: a free particle couples to a heat bath through a friction force whose sign and strength adjust to keep the time-average of the square of the velocity equal to the square of the thermal velocity $\bar{v}$. The system has a single time constant τ_0 that measures the strength of coupling between the particle and the heat bath. The time variation of all the relevant physical variables can be scaled to this quantity, with the associated spatial dependencies being scaled to an effective length $l = \bar{v}\tau_0$. Depending on the various physical scenarios, this length can be interpreted as a scattering length or a mean free-path for collision with another particle or structure.

Because of the underlying Hamiltonian formalism and low dimensionality, the motion of a free particle in the NH model is integrable, resulting in closed, periodic orbits in the relevant phase-space. Although the orbits are nonlinear and intermittent, the non-chaotic particle motion is unidirectional, non-diffusive, and the velocity distribution function is far from being a Maxwellian; a particle initially at rest always remains at rest. However, the majority of the applied studies incorporate the action of an external potential $\phi(r)$ because that is the typical environment of relevance to a physical system. The inclusion of such a potential enlarges the dimensionality of the phase-space, and while retaining the Hamiltonian structure, the dynamics now has access to a chaotic sea that allows the behavior, over limited parameter regimes, to display a more thermal character. But it must be recognized that it is the interaction between ϕ and the reservoir that causes the quasi-thermalization, and that path requires the presence of a chaotic environment.

Several researchers [12-17] have recognized the need to enlarge the original NH model to better approximate a thermal interaction, yet remaining faithful to the deterministic thermostat philosophy. In one method or another, the various additions to the NH model seek to enhance the role of chaotic dynamics. A necessary ingredient is the increase in the dimensionality of the associated phase-space. To this end, some approaches increase the

number of the heat reservoirs, in a cascading order, while adhering to the coupling through a frictional force. Some studies also introduce higher (odd) powers of the velocity to augment the frictional force. Typically, the multiple reservoirs are studied in conjunction with ϕ and found to result in a more satisfactory thermal character than the simple NH model. But again, it is the interaction between the potential and the reservoirs that achieves the result.

Another approach [18,19] to introduce chaotic behavior into deterministic thermostats is to include external forces whose temporal dependence is chosen, a priori, to resemble the behavior of a Langevin-type of force, but having an explicit deterministic origin. The merit of this methodology is that the chaotic behavior transforms fractal-type distributions into smooth, Maxwellian-like functions, in the absence of ϕ. Also, the resulting orbits resemble the Brownian motion expected for a free particle interacting with a heat reservoir. The present study adheres to this general concept while retaining the inherent simplicity of the NH model.

This manuscript presents a numerical investigation of the properties of a free particle interacting with a deterministic reservoir in which a new Langevin-type of force is included, but its time dependence is not a-priori determined. The force is linked directly to the evolution of the self-consistent damping coefficient associated with coupling to the heat bath. The resulting behavior displays features characteristic of coupling to a thermal reservoir, such as self-heating and diffusive behavior. For overall perspective and motivation for the focus of the present work, it should be mentioned that the lack of diffusive behavior has been previously identified to be a shortcoming of deterministic thermostats, and remedies have been found by increasing the number of degrees of freedom [20, 21].

At the outset of this type of investigation it is appropriate to ask what is the merit of pursuing chaotic behavior at the single particle level. After all, by adding many particles to a system may by itself cure the lack of chaos in a heuristic and practical sense, and may be suitable in a variety of applications. But there is always the concern of whether or not the behavior sampled is correct at the basic level. This issue is of particular significance in studies of thermal systems that are externally driven. For example, a particle in a thermal system interacting with a wave. The wave-induced modification of an individual chaotic orbit can lead to consequences unrelated to the global chaos possibly induced by the consideration of many particles.

The manuscript is organized as follows. Section II describes the model investigated.

Section III presents numerical results including, self-heating, correlations, spectral features, diffusion, and response to an external force. It also compares the behavior of the Nosé-Hoover thermostat to that developed by Martyna et al. Conclusions are given in Sec. IV.

II. MODEL

The equations for the proposed extension of the basic NH model have the form (in one-dimension)

$$m\frac{dv}{dt} = F(t) - \gamma(t)mv, \tag{1}$$

$$\frac{d\gamma}{dt} = \tau_0^{-2}\left[\left(\frac{v}{\bar{v}}\right)^2 - 1\right], \tag{2}$$

where t is the physical time in seconds, m is the particle mass, v the velocity, F the fluctuating force, γ the damping coefficient, τ_0 the coupling time between the particle and the reservoir, and $\bar{v}$ the thermal velocity.

The choice of the force F is guided by the fact that it should have zero mean, have a short autocorrelation, and be related self-consistently to the reservoir. The following expression satisfies such constraints

$$F = F_0 \sin(\theta), \tag{3}$$

$$\frac{d\theta}{dt} = \gamma(t), \tag{4}$$

with F_0 the peak strength of the fluctuating force. The natural scaling of this system results in the scaled variables used in the numerical study,

$$u = \frac{v}{\bar{v}}, \quad \tau = \frac{t}{\tau_0}, \quad \Gamma = \gamma\tau_0, \quad \lambda = \frac{F_0\tau_0}{m\bar{v}}, \quad \eta = \frac{x}{\bar{v}\tau_0}, \tag{5}$$

in which x is the physical position (e.g., in cm) and η the scaled position.

The scaled system becomes

$$\frac{du}{d\tau} = \lambda \sin(\theta) + \Gamma u, \tag{6}$$

$$\frac{d\Gamma}{d\tau} = u^2 - 1, \tag{7}$$

$$\frac{d\theta}{d\tau} = \Gamma. \tag{8}$$

The system defined by the choice $\lambda = 1$ has been found, after numerical surveys, to provide the best description for a free particle in contact with a heat bath.

In making later comparisons between the single NH thermostat and the dual MKT thermostat, a parameter h is included, with the system of Eqs. now taking the form

$$\frac{du}{d\tau} = \frac{\sin(\theta) + h\sin(\alpha)}{1+h} - \Gamma u, \tag{9}$$

$$\frac{d\Gamma}{d\tau} = u^2 - 1 - h\Gamma\xi, \tag{10}$$

$$h\frac{d\xi}{d\tau} = h(\Gamma^2 - 1), \tag{11}$$

$$\frac{d\theta}{d\tau} = \Gamma, \tag{12}$$

$$h\frac{d\alpha}{d\tau} = h\xi, \tag{13}$$

in which the choice $h = 1$ corresponds to the MKT model, and $h = 0$ recovers the NH model.

In writing the fluctuating force in Eq. (9), the principle has been followed that each thermostat generates an explicitly uncorrelated force, although correlations develop through the coupling to each of the thermostats. Another obvious possibility for the dual force associated with the MKT model is of the form $\sin(\theta+\alpha)$, which has also been explored, but due to the explicit phase correlations that can appear, the thermal character of the particle motion is not as good as that obtained with the additive expression in Eq. (9).

The system defined by Eqs. (9)-(13) has an effective energy function

$$U = \frac{u^2}{2} + \frac{\Gamma^2}{2} + \frac{h\xi^2}{2} + \theta + h\alpha, \tag{14}$$

and a corresponding conservation of energy Eq.

$$\frac{dU}{d\tau} = u\left(\frac{\sin(\theta) + h\sin(\alpha)}{1+h}\right), \tag{15}$$

in which the RHS shows the power exchanged between the particle and the reservoirs through the fluctuating force. In general the reservoirs start interacting with the particle with unknown phases that are equally probable, (θ_0, α_0). In the numerical results shown in Sec. III averages over these initial phases are made, which from Eq. (15) correspond to

$$\left\langle \frac{dU}{d\tau} \right\rangle = 0. \tag{16}$$

The chaotic dynamics is governed by the nonlinear interplay (e.g., frequency mixing, harmonics, half-harmonic generation) of several characteristic frequencies and decay-times

that are embedded in various sub-elements of the system of Eqs. (9)-(13). These frequencies appear later when examining spectral features in Figs. 7. They can be extracted by analyzing the linear response about possible stationary points, i.e., for a stationary value g_0 associated with a given variable g the linear response is written as $g = g_0 + \tilde{g}e^{s\tau}$, where the complex exponent s is one of the eigenvalues of the corresponding system determinant, and $\tilde{g}$ a constant initial value. Next, the relevant eigenvalues are identified.

It is evident from Eqs. (11) and (12) that for $h = 1$, the fluctuation-MKT model does not have a global stationary point, but for $h = 0$, the fluctuation-NH system does. The associated stationary points are:

$$\Gamma_0, \quad u_0 = \pm 1, \quad \theta_0 = n\pi \quad \text{with} \quad n = 0, 1... \tag{17}$$

The corresponding (cubic) eigenvalue Eq. is

$$s^3 + 2u_0(u_0 s - \cos\theta_0). \tag{18}$$

Choosing each of the appearances of the factor u_0 to have the same value results in two equations

$$s^3 + 2(s \pm 1) = 0. \tag{19}$$

The two signs in Eq. (19) generate eigenvalues that are the negative of each other; they simply represent time going forward or backward, but the numerical values are the same. The numerical values of the three roots for the positive sign in Eq. (19) are

$$0.3855 \pm i1.5639, -0.7709. \tag{20}$$

As is shown later in Fig. 7, the numerical solution of the nonlinear dynamics indicates that the frequency labeled $a = 1.56$, found from Eq. (19), appears prominently. But surprisingly, it is also seen later in Fig. 7 that another frequency, labeled $c = 0.59$, plays a key role in shaping the spectra. This frequency does not correspond to the standard eigenvalues in Eq. (19). What is peculiar is that this other frequency corresponds to one of the eigenvalues of the expression obtained from Eq. (18) when each of the factors u_0 are allowed to attain their stationary points separately. This split choice generates the pair

$$s^3 - 2(s \pm 1) = 0. \tag{21}$$

In analogy to Eq. (19) the two signs correspond to the time-reversal solutions. For the positive sign in Eq. (21) the numerical values of the corresponding three roots are

$$-0.8846 \pm i0.5897, 1.7693. \tag{22}$$

There are two other frequencies that are present in the dynamics and which appear in the spectra shown later in Fig. 7. One is the ubiquitous frequency for velocity oscillations about the equilibrium value $u_0 = \pm 1$ for a free particle in contact with the NH thermostat, labeled $b = \sqrt{2}$. The other arises from the eigenvalues associated with only the fluctuating force, in the absence of the friction term in Eq. (6), but still with the phase advance determined by the contact to the NH heat bath in Eq. (8). In this limit, the eigenvalues are obtained from the characteristic Eq. $s^3 = \pm 2$, namely $(\pm 0.63 \pm i1.09, \pm 1.26)$, which identifies the other hidden frequency in the dynamics, labeled $d = 1.09$.

Before examining the numerical solution of the model equations it is worth emphasizing that the new force term preserves the time-reversal properties intrinsic to the NH and MKT thermostats. Also, no stochasticity is explicitly introduced by the new force term. The chaotic behavior to be illustrated in the following section is thus a manifestation of 'deterministic chaos'.

III. NUMERICAL RESULTS

The numerical results presented in this section are obtained by solving Eqs. (9)-(13) with a fourth-order Runge-Kutta method using a time step $dt = 10^{-3}$, as is typical of studies of this subject. Characteristically, the calculations are stored every 20 steps for further analysis, for a total time record of $\tau = 5,000$. When performing phase-averages, 200 values of θ_0 , and 50 values of α_0, distributed uniformly in $(0, 2\pi)$, are sampled.

A. Self-heating

For thermostat models in which only a friction force is present, as in the NH and MKT systems, a free particle whose initial velocity is zero remains at rest forever. To explore heating-related issues in those systems, a range of non-zero initial velocities must be considered. That is not the case in the present model because the fluctuating force provides an

effective "zitterbewegun" that allows a single, initially stationary particle to self-heat. The nature of this trembling motion in the absence of the usual friction force in the equation of motion, Eq. (9), but retaining the coupling to the thermostats, has been investigated in detail. But for brevity the corresponding figures are not shown.

It is found that without the friction term the behavior is quite different for the two thermostats. In the case of NH, there is a very rapid transient in the large time-scale and is followed by a nearly constant velocity. The reason for this behavior is that Eq. (10), for $h = 0$, results in the damping coefficient increasing linearly in time, and thus the phase-angle advances as $\theta \sim \tau^2$ which causes the fluctuating force to oscillate rapidly. Effectively, as time increases the particle enters an inertial regime in which the oscillations are very small compared to the mean velocity. The MKT system exhibits a behavior more typical of chaotic dynamics, as expected from the inclusion of an extra degree of freedom, i.e., two heat baths that communicate with each other. For MKT the reservoirs develop a self-consistent locking that results in relatively slow oscillations of the effective fluctuating force, compared to that in the NH model.

For both the NH and MKT models the combined action of the fluctuating force and the friction force causes a particle to execute non-periodic oscillations in the positive and negative directions. The magnitude of the velocity swings is bounded to the range $|u| \leq 4$, with the MKT model displaying more, lower-frequency structures, than the NH model. Figure 1 shows the chaotic phase-space, (Γ, u), formed by the velocity and the damping coefficient, under the combined action of the fluctuating force and the friction force. The figure displays only points sampled after 100 computation steps. It is seen from Fig. 1 that the use of two reservoirs in the MKT model results in a more dense, and symmetric, population of the phase-space than in the NH model.

The approach to equilibrium by a single particle initially at rest, with initial phases $\theta_0 = 0$, $\alpha_0 = 0$, and coefficients $\Gamma(0) = 0$, $\xi(0) = 0$ has been analyzed (but not shown) by examining the time dependence of the running, time-average of the square of the scaled velocity

$$\langle u^2 \rangle_\tau = \frac{1}{\tau} \int_0^\tau ds \left(u(s) \right)^2 . \tag{23}$$

It is found that the NH model approaches the expected value, $\langle u^2 \rangle_\tau = 1$ on a time scale of $\tau \approx 250$, more rapidly than the MKT model, which displays a relaxation time close to $\tau \approx 1500$.

To complement the information about the self-heating, Fig. 2 presents an example of the time dependence of the self-consistent, fluctuating force for the MKT model, top panel a), and the NH model, bottom panel b). Note that the time interval shown, $0 < \tau < 100$, is small compared to that sampled in Fig. 1.

B. Correlations

The behavior of the velocity autocorrelation function

$$C_u(\tau) = \frac{\int_0^T ds\ u(s+\tau)u(s)}{\int_0^T ds\,(u(s))^2}, \tag{24}$$

is examined for the choice of the maximum time, $T = 5000$, corresponding to the entire time interval displayed in Fig. 1.

Figure 3 illustrates the effect of the fluctuating force on the velocity correlations associated with the NH and the MKT models. To make this comparison it is necessary to start with a non-zero initial velocity, taken here as $u(0) = 0.5$. The top (blue) curve in both panels corresponds to the velocity autocorrelation function with only the frictional force affecting the particle motion. It is evident that both of these systems are strongly correlated, as is well known. The bottom (red) curves on both panels show the autocorrelation functions when the fluctuating force is activated. It is seen that the correlations are effectively destroyed over times $\tau > 10$, with the NH model displaying a shorter de-correlation, time-scale than the MKT model.

C. Frequency spectra

Insight about the dynamical processes is obtained from the features of the frequency spectrum. In generating the various spectra from the numerical time series, a Hanning window is applied.

The top panel a) of Fig. 4 shows the time evolution of the scaled velocity for the NH model over a short time interval, $600 < \tau < 700$. The striking feature is the appearance of large, narrow pulses, embedded in much slower oscillations, with their appearance time, τ_j, seemingly random. The black curve is the numerical solution, and the red curve is an

analytical, Lorentzian-function, centered on one of the pulses, i.e.,

$$L(\tau) = \frac{A\tau_L^2}{(\tau - \tau_j)^2 + \tau_L^2}, \tag{25}$$

in which A represents the peak amplitude of a pulse, and τ_L its width. For the pulse selected at $\tau_j = 629.6$, A is adjusted to match the peak, and $\tau_L = 0.51$. The bottom panel b) of Fig. 4 shows the isolated pulse on an expanded time-scale; it is seen that the shape of the pulse is indeed a Lorentzian function. The deviation between the black and the red curve for large time differences arises because the pulse is embedded in lower-frequency oscillations.

The significance of the Lorentzian shape of the pulse is that the corresponding frequency spectrum has an exponential dependence on the frequency f

$$\tilde{L}(f) = \pi A \tau_L e^{-2\pi\tau_L f} e^{i2\pi\tau_L f}. \tag{26}$$

For a dynamical system in which the distribution of widths is narrow, and the appearance of the pulses is weakly correlated, as is typical of chaotic phenomena, a distinct signature is an exponential frequency dependence for the ensemble average of the amplitude of the frequency spectrum of the relevant physical variable, say S,

$$\left\langle \left| \tilde{S}(f) \right| \right\rangle \propto e^{-2\pi\tau_L f}. \tag{27}$$

The broadband spectra of the classic models of chaotic systems have been shown in the numerical studies by Ohtomo et al. [22] to follow such an exponential dependence. Basic laboratory studies of heat transport in plasmas [23] have measured the individual Lorentzian pulses and identified that they are the cause of the associated exponential spectra, and of the chaotic behavior [24]. A related analytical study [25] has demonstrated the origin of such unique pulses. They are the ubiquitous flights around fixed points in the underlying phase space; their width is determined by the associated linear eigenvalues.

Figure 5 shows a segment of the phase-space evolution of the variables (Γ, u) associated with Fig. 4, and corresponding to the NH model. The more complex blue trajectories arise from the interval displayed in the top panel a) of Fig. 4. The thicker red curve highlights the trajectory that belongs to the Lorentzian pulse shown in the bottom panel b) of Fig. 4. It is evident from this display that the sharp, intermittent pulses are rapid, Lorentzian flights around the quasi-stationary fixed points $\Gamma = 0$, $u = \pm 1$.

Figures similar to 4 and 5 have been generated for the MKT model but for brevity are not shown. They demonstrate that the MKT model displays the same dynamical behavior as

the NH model, as expected for a chaotic system. It exhibits the characteristic intermittent pulses, Lorentzian shape, and rapid phase-space flights. The Lorentzian width for a typical MKT pulse is $\tau_L = 0.57$. The conclusion drawn from such analysis is that the fluctuating force transforms the NH and MKT thermostats into intrinsically chaotic systems.

It should be noted that the results shown in Figs. 4 and 5 pertain to a single particle started with zero velocity, and zero starting phases, as is necessary to study a representative trajectory that undergoes self-heating by the fluctuating force. The features to be examined next are ensemble averages over the initial phases, but keeping the initial velocity equal to zero.

Figure 6 displays the ensemble average of the amplitude of the velocity spectrum for the NH model. The scaled frequency in the figure is the frequency f. The left panel uses a log-linear format, and the right panel a log-log format, as is typically done in turbulence studies. The purpose of using the two displays is to illustrate that the multiple power-laws apparent in the log-log display, which could suggest misleading interpretations, are nothing but an exponential dependence resulting from the Lorentzian pulses. The dark blue curves are obtained from the numerical solution, and the red curves are exponentials given by Eq. (27), for a value $\tau_L = 0.54$, while the fit to a single-phase, isolated pulse, shown in Fig. 4, is $\tau_L = 0.51$. It is also evident that the broadband base of the spectrum described by Eq. (27) is punctuated by large amplitude, coherent peaks of relatively low frequency.

Figure 7 focuses on the low-frequency features of Fig. 6, using a linear display. The dark blue curve is obtained from the numerical solution. There are 3 red vertical lines acting as markers corresponding to the angular frequencies: $a = 1.56$, $b = \sqrt{2}$, $c = 0.59$. These angular frequencies have been previously identified in Sec. II. 'a' is the magnitude of the imaginary part of the complex root in Eq. (20), 'b' is the angular frequency of a free particle without the fluctuating force, and 'c' is the magnitude of the imaginary part of the complex root in Eq. (22). The arrows connecting to the various peaks indicate the combinations of these basic frequencies that are responsible for their appearance. It is clear that the fluctuating force allows for non-trivial, frequency-coupling channels to be excited. These features may be manifestations of properties previously identified with strange non-chaotic attractors [26-28]. It is emphasized that analogous results to those shown in Figs. 6 and 7 have been obtained for the MKT model but for brevity are not shown. The MKT model also displays the characteristic exponential frequency dependence with a characteristic value

$\tau_L = 0.54$, while the fit to a single-phase, isolated pulse has $\tau_L = 0.57$. However, it is to be noted that the frequency combinations leading to coherent peaks are different. For the MKT model the largest peak appears at an angular frequency equal to $c/2$, the second largest is at an angular frequency equal to $d = 1.09$, and a smaller peak is discernable at an angular frequency equal to $9c/2$.

D. Distributions

Distribution functions for a given quantity are constructed from the numerical solutions by binning within 41 bins, the values attained over 50,000 stored time-steps, for a given initial phase. The phase-averaged distributions are generated by adding the individual distributions for an ensemble of initial phases.

The left panel a) of Fig. 8 displays the phase-averaged, velocity distribution functions for the MKT and NH models, in a linear scale. It is seen that the NH model (black curve) has a deficit of low-velocity particles and, as a consequence, is a bit wider at the waist. In contrast, the MKT model (red curve) has a rounded, over-populated, group of low-velocity particles. The right panel b) shows the phase-averaged distribution of the associated damping coefficient Γ. The MKT (red curve) does show a much closer approximation to a Maxwellian distribution, with the peak looking more parabolic. However, the NH model (black curve) shows significant departures, notably, it seems to have a net, positive bias. To some extent the variations of the NH model are enhanced over those of the MKT model due to the smaller ensemble sampled (50 times smaller).

Figure 9 presents a log-linear display of the distribution functions for the MKT model. The left panel is the velocity distribution function, and the right panel the Γ-distribution. The blue crosses are the individual numerical values calculated and the red curve is an analytic Maxwellian distribution for $\bar{u}^2 = 1$. The fit for the damping coefficient is quite close to a Maxwellian, but the velocity distribution does show a more square behavior at low velocities.

E. Diffusion

The diffusive behavior is examined by constructing the running, time-average of the square of the (scaled) particle position, $\eta = x/l$, for a given initial phase,

$$\left\langle \eta^2 \right\rangle_\tau = \frac{1}{\tau} \int_0^\tau ds \left(\eta(s)\right)^2 \tag{28}$$

The phase-averaged, square displacement is generated by adding the individual results of Eq. (28) for an ensemble of individual phases.

To compare the scaled numerical results to the Einstein relation, use is made of the standard definitions for the diffusion coefficient D and the mobility μ

$$\langle x^2 \rangle = 2Dt, \quad \langle v \rangle = \mu G, \tag{29}$$

for an applied constant force G to a particle undergoing Brownian motion. With the scaling defined in Eq. (5), the Einstein relation is connected to the quantities that can be numerically evaluated, namely,

$$\frac{D}{\mu T} = \frac{\langle \eta^2 \rangle / 2\tau}{\langle u \rangle / E}, \tag{30}$$

where E now represents the additional, scaled, constant-force to be added to the system of Eqs. (9)-(13) used in the numerical solution, and T is the temperature of the heat bath. The Einstein relation states that the ratio on the right-hand side of Eq. (27) is unity.

Figure 10 displays the time dependence of the average of the square displacement for the MKT (red curve) and the NH (black curve) models. The blue, straight-lines are fits to the numerical results to illustrate that the self-consistent, fluctuating force induces diffusive behavior on a free particle for both models. The scaled diffusion coefficient for the MKT model is 1.45, and 0.69 for the NH model, roughly different by a factor of 2.

To extract the mobility coefficient, a pulsed force is applied. The reason is that this is a dynamical system with an inherent inertia. It takes a finite time to reach a steady-state for a given strength of the applied force. If the force is too large, the system runs away and enters a ballistic regime. If the force is too small, the fluctuations overwhelm the small induced velocity, i.e., it is below the noise-floor. Thus, only a narrow range of values of E result in a valid test of the Einstein relation. An example is illustrated for the NH model in Fig. 11. In this case $E = 0.049$. The red curve shows the time evolution of the mobility induced by the temporal pulse shown; it has a top-hat shape over the interval $300 < \tau < 2500$. After a

transient stage, the mobility tends toward a steady value of 0.56. After the pulse is turned-off, the average velocity experiences a slow decay. A similar behavior is also obtained for the MKT system (not shown). For this other model an applied force of strength $E = 0.03$ yields a steady mobility value of 0.76.

Defining the right-hand side of Eq. (30) as the Einstein ratio, the results shown in Figs. 10 and 11 yield a value of 1.23 for the NH model, and 1.81 for the MKT model. For the NH model it is found that an additional velocity average over 11 initial values, $u(0)$, ranging over $-4 < u(0) < 4$ results in an Einstein ratio of 1.07. Thus, within the statistical uncertainty, the behavior of the NH model can be said to agree quantitatively with the Einstein relation.

Figure 12 illustrates the transition from diffusive to ballistic behavior for the NH model for an applied force $E = 0.035$. The black curve is the time evolution of the averaged, squared-displacement; it is the diffusive behavior shown earlier in Fig. 10 in the absence of an external pulse. The red curve is the behavior when the pulse shown at the bottom of the figure is activated. It is seen that while the pulse is 'on' the displacement increases quadratically (or slightly faster). But when the pulse is turned-off, the particle returns to the diffusive behavior induced by the fluctuating force. The two blue, straight-lines, have the same slope, equal to that fitting the behavior of the NH model in Fig. 10.

IV. CONCLUSIONS

This study has shown that the inclusion of a self-consistent, fluctuating force into the dynamical equation transforms the NH and MKT deterministic thermostats into 'deterministic chaotic systems'. The fluctuating force is linked to the damping coefficient that connects the particle velocity to the heat bath. In a sense, this addition better mimics a physical situation in which a free particle embedded in a thermal environment experiences both, a complicated force with zero-mean value, and also friction. But, physically, the fluctuating force and the damping have the same deterministic origin, namely, the interaction with the larger elements that constitute the heat bath. In the simplest model considered here this interaction is summarized by two parameters: the thermal velocity $\bar{v}$, and the coupling time-constant to the heat bath τ_0. Using these quantities to scale the dependent and independent variables yields a universal system, that, in principle, is relatively simple.

The consequences of the fluctuating force have been investigated numerically for two

well-known deterministic thermostats: the Nosé-Hoover (NH) model, and the Martyna-Klein-Tuckerman (MKT) model. A significant improvement on both models caused by the fluctuating force is that the velocity autocorrelation function decays rapidly. As a result, it is found that for both models the additional force induces diffusive motion for an initially stationary particle, with the MKT model displaying a diffusion coefficient $D \approx 1.45\bar{v}^2\tau_0$, which is approximately a factor of 2 larger than that for the NH model. The application of an external constant force results, within a limited range of the strength of the applied force, in a value for the mobility coefficient that for the NH model is quantitatively equal, within statistical uncertainty, to that predicted by the Einstein relation. For the MKT model the value is a factor of 2 larger. This discrepancy conjures the possibility that its remedy may be achieved by increasing the number of thermostat variables in the MKT system. This is an intriguing question whose answer requires a dedicated study.

The fluctuating force results in a velocity distribution function for the MKT model that comes close to being a Maxwellian, except for an increase in the low velocity particles. For the NH model the chaotic fluctuations induce a significant decrease in the number of low-velocity particles, resulting in a wider waist. But the distribution function for the damping coefficient that couples to the heat bath shows a remarkable good fit to a Maxwellian function for the MKT model. For the NH model, it shows significant departures from a Maxwellian. These comparisons suggest that the chaotic extension of the MKT thermostat provides a closer approximation to thermal behavior within a purely deterministic description.

For both thermostat models the fluctuating force causes the spectra of all (not all shown here for brevity but have been individually verified) the relevant variables to exhibit the characteristic exponential frequency dependence associated with chaotic systems. It has been demonstrated that such spectra are the consequence of intermittent, sharp pulses that have a unique Lorentzian shape. Topologically, the pulses correspond to rapid flights around quasi-stationary points in the (Γ, u) phase-space. This explicit finding has dual implications. In the context of the present work, it demonstrates that the fluctuating force results in a self-consistent chaotic system, i.e., it transforms a deterministic thermostat into a 'deterministic chaotic thermostat'. From the point of view of the study of chaotic dynamics, the results shown provide new examples of dynamical systems in which the connection between Lorentzian pulses and exponential frequency spectra has been established [29, 30]. However, since the spectra of Fig. 6 indicates that coherent features are also present, the

system does not achieve a state of complete chaos. Thus, it seems worthwhile to pursue in a future study the connection of the 'degree of chaos' to parameter tuning by using various mathematical measures of chaos.

In summary, a chaotic extension of deterministic thermostats is found to better approximate the interaction of a classical particle with a heat bath. Future studies of more complex situations in which the fluctuating force is included appear to be worth pursuing.

ACKNOWLEDGMENT

This work is performed under the auspices of the Basic Plasma Science Facility (BaPSF) at the University of California, Los Angeles (UCLA), which is jointly supported by a DOE-NSF cooperative agreement. The author thanks Mr. M. Poulos for valuable help in the preparation of the manuscript.

---

[1] S. Nosé, J. Chem. Phys. 81, 511 (1984).

[2] Wm. G. Hoover, Computational Statistical Mechanics, Elsevier, Amsterdam (1991).

[3] D. J. Evans and G. P. Morris, Statistical Mechanics of Nonequilibrium Liquids, Academic Press, New York (1990).

[4] G. P. Morris and C. P. Dettman, Chaos 8, 321 (1998).

[5] Ch. Dellago, L. Glatz, and H. A. Posch, Phys. Rev E 52, 4817 (1995).

[6] K. Rateitschack, R. K. Klages, and W. Hoover, J. Stat. Phys. 101, 61 (2000).

[7] Wm. G. Hoover, K. Aoki, C. G. Hoover, and S. V. DeGroot, Physica D 187, 253 (2004).

[8] O. G. Jepps and L. Rondoni, J. Phys. Math, A: Math. Theor. 43, 133001 (2010).

[9] K. W. Myerscough, J. Frank, B. Leimkuhler, Proc. R. Soc. A 473, 20160730 (2017).

[10] D. Kusnezov, A. Bulgac, and W. Bauer, Annals of Physics 2014, 155 (1990).

[11] W. G. Hoover, Phys. Rev. A 31, 1695 (1985).

[12] G. J. Martyna, M. L. Klein, and M. Tuckerman, J. Chem. Phys. 97, 2635 (1992).

[13] A. Bulgac and D. Kusnezov, Phys. Rev. A 42, 5045 (1990).

[14] N. Ju and A. Bulgac, Phys. Rev B 48, 2721 (1993).

[15] Wm. G. Hoover and B. L. Holian, Phys. Lett. A 211, 253 (1996).

[16] P. K. Patra and B. Bhattacharya, J. Chem. Phys. 140, 064106 (2014).

[17] P. K. Patra, J. C. Sprott, Wm. G. Hoover, and C. G. Hoover, Molecular Physics 113, 2863 (2015).

[18] C. Beck, Physica A 233, 419 (1996).

[19] M. Mackey and M. Tyran-Kaminska, Physics Reports 422, 167 (2006).

[20] A. Bulgac and D. Kusnezov, Phys. Lett. A, 151, 122 (1990).

[21] G. Huerta-Cuellar, E. Jimenez-Lopez, E. Camos-Canton, and A. N. Pisarchik, Commun. Nonlinear Sci. Numer. Simulat. 19, 2740 (2014).

[22] N. Ohtomo, K. Tokiwano, Y. Tanaka, A. Sumi, S. Terachi, and H. Konno, J. Phys. Soc. Jpn. 64, 1104 (1995).

[23] D. C. Pace, M. Shi, J. E. Maggs, G. J. Morales, and T. A. Carter, Phys. Plasmas 15, 122304 (2008).

[24] J. E. Maggs and G. J. Morales, Plasma Phys. Control. Fusion 55, 085015 (2013).

[25] J. E. Maggs and G. J. Morales, Phys. Rev. E 86, 015401 (2012).

[26] C. Gribogi, E. Ott, S. Pelikan, and J. A. Yorke, Physica D 13, 261 (1984).

[27] F. J. Romeiras and E. Ott, Phys. Rev. A 35, 4404 (1987).

[28] A. S. Pikovsky and U. Feudel, Chaos 5, 253 (1995).

[29] J. E. Maggs and G. J. Morales Phys. Rev. Lett. 107, 185003 (2011).

[30] O. E. Garcia and A. Theodorsen, Phys. Plasmas 24, 020704 (2017).

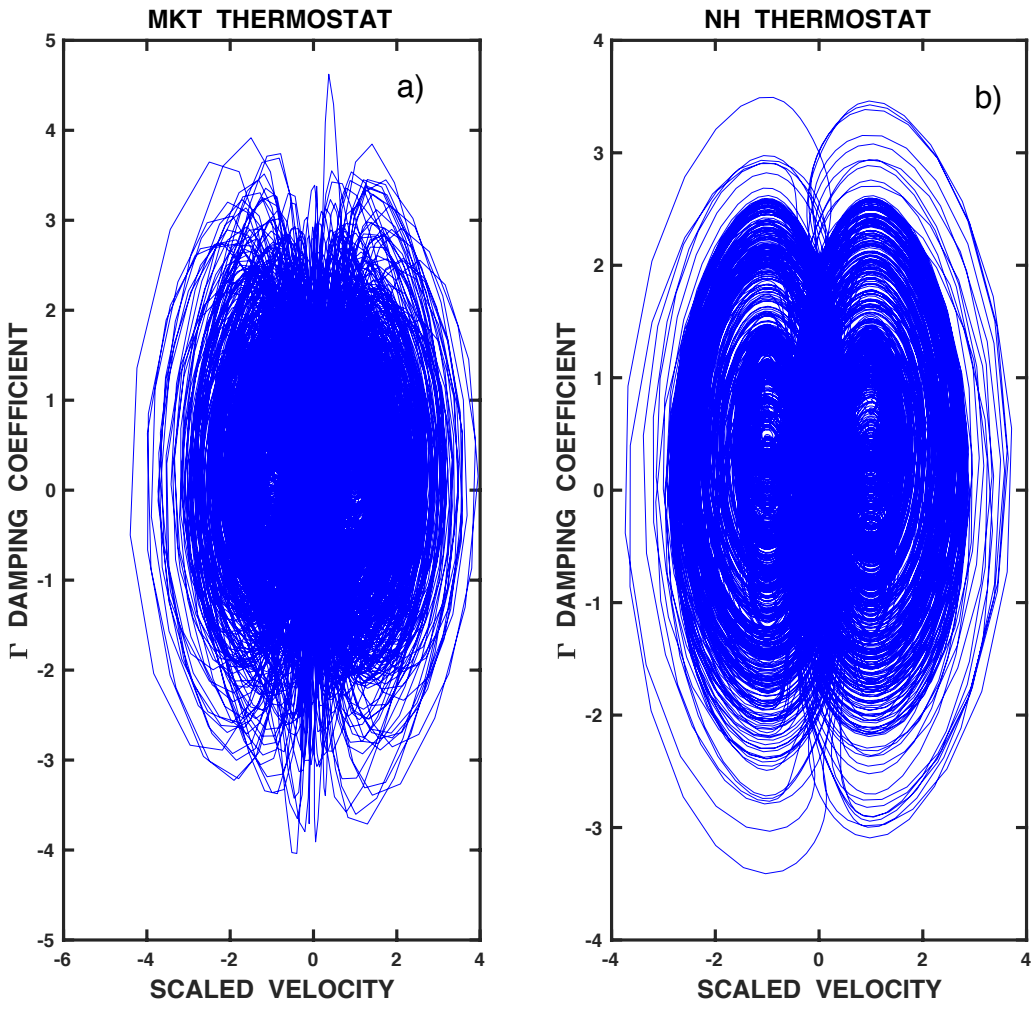

FIG. 1. (Color on line) Chaotic phase-space (Γ, u) generated when the fluctuating force and damping force act together for the MKT model (left panel) and NH model (right panel) for a particle initially at rest. Display shows points sampled after 100 computational steps over the time interval $0 < \tau < 5000$.

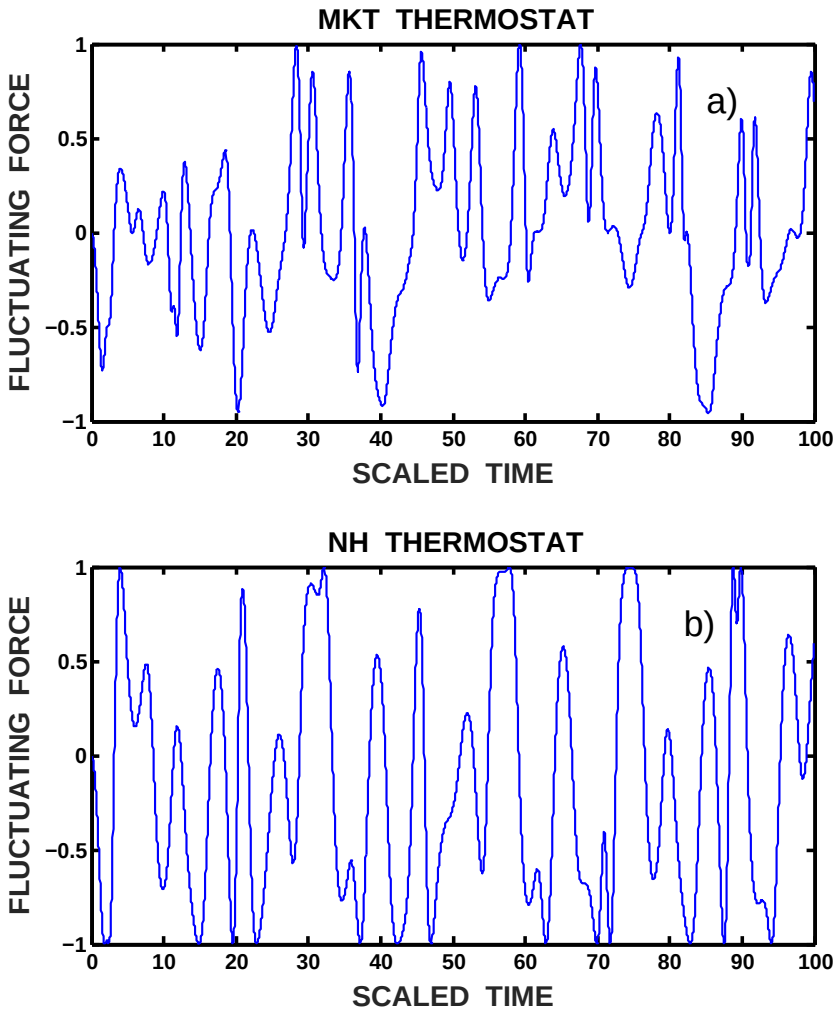

FIG. 2. (Color on line) Typical time dependence of the self-consistent, fluctuating force for a) the MKT model, and b) the NH model. Note the small time interval shown, $0 < \tau < 100$, in comparison to that in Fig. 1.

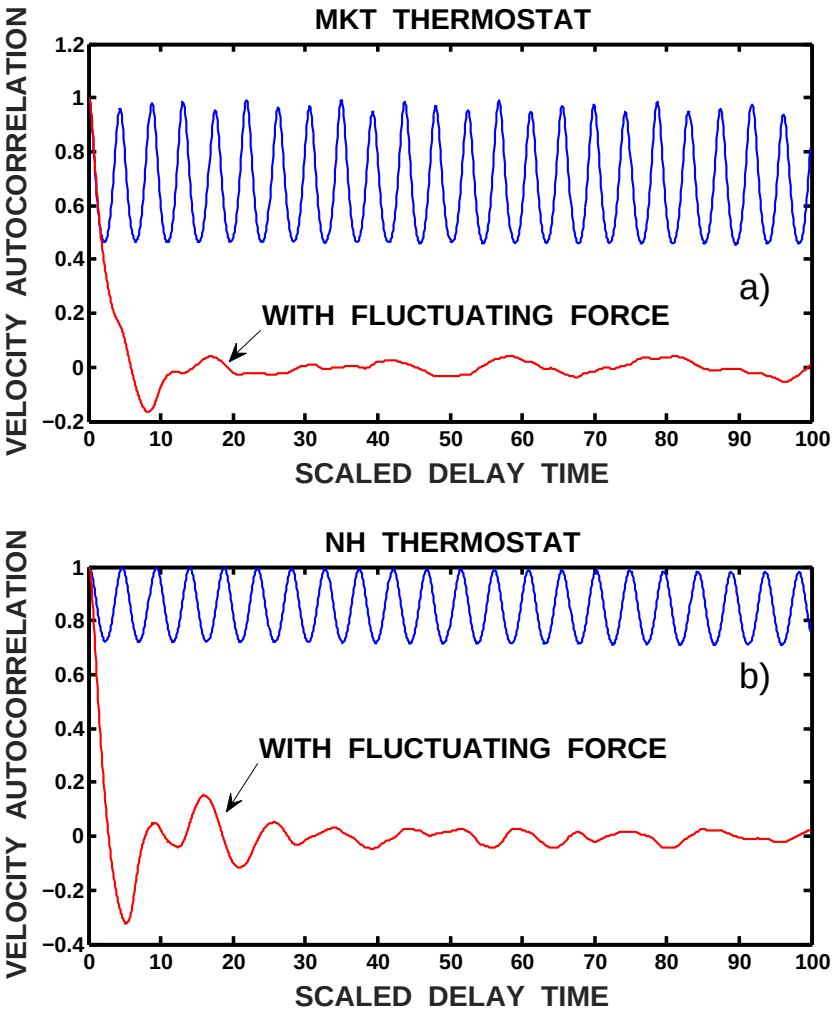

FIG. 3. (Color on line) Effect of fluctuating force on the velocity autocorrelation function for a particle with an initial scaled-velocity $u = 0.5$ for: a) MKT model, and b) NH model. The top blue curve in each panel only includes the frictional force. The bottom red curves show the decay of the correlation when the fluctuating force is included.

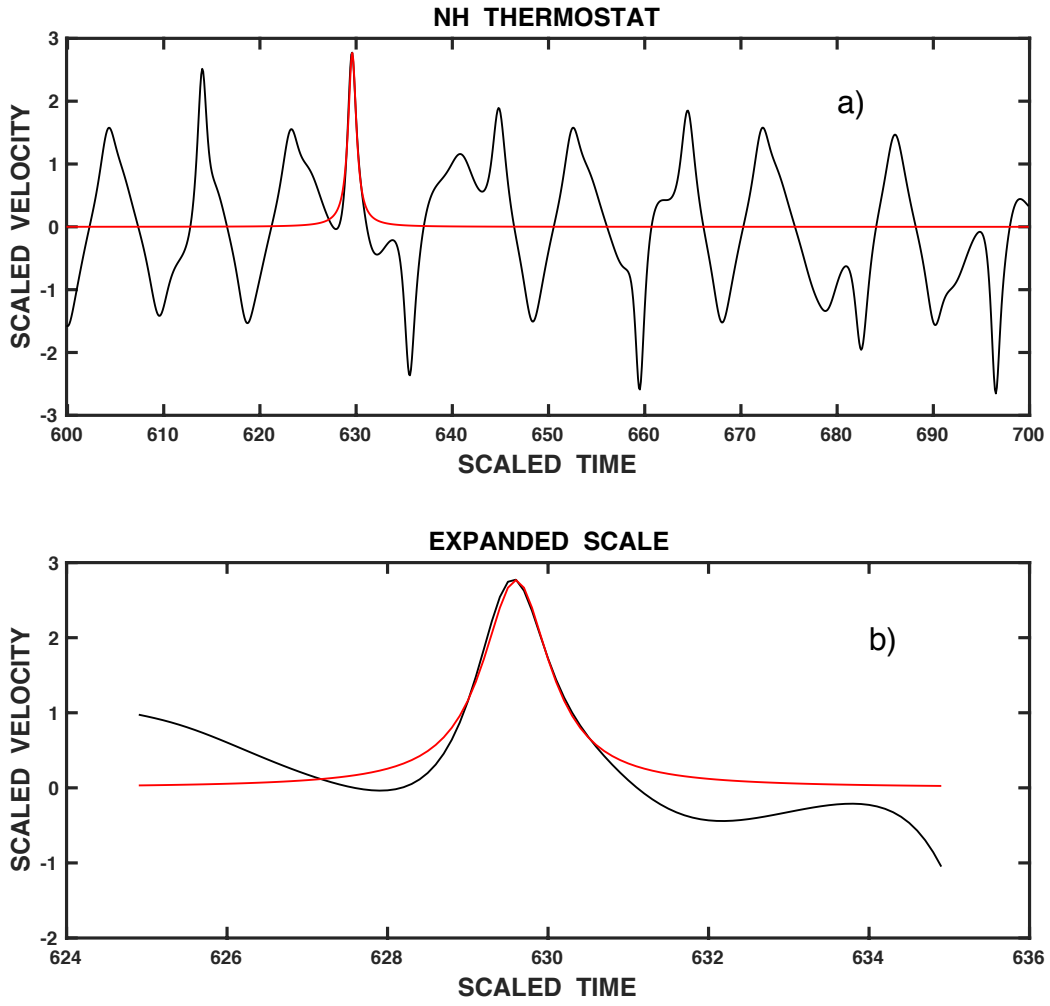

FIG. 4. (Color on line) Small-scale temporal structure of the scaled velocity in the NH model. Top panel a) displays the interval, $600 < \tau < 700$, during which several sharp pulses are present. Superposed on the black time-trace is a red curve consisting of a Lorentzian function chosen to line-up with one pulse. The bottom panel b) shows an expanded view. The width of the Lorentzian is $\tau_L = 0.51$. Similar results are obtained for the other narrow pulses.

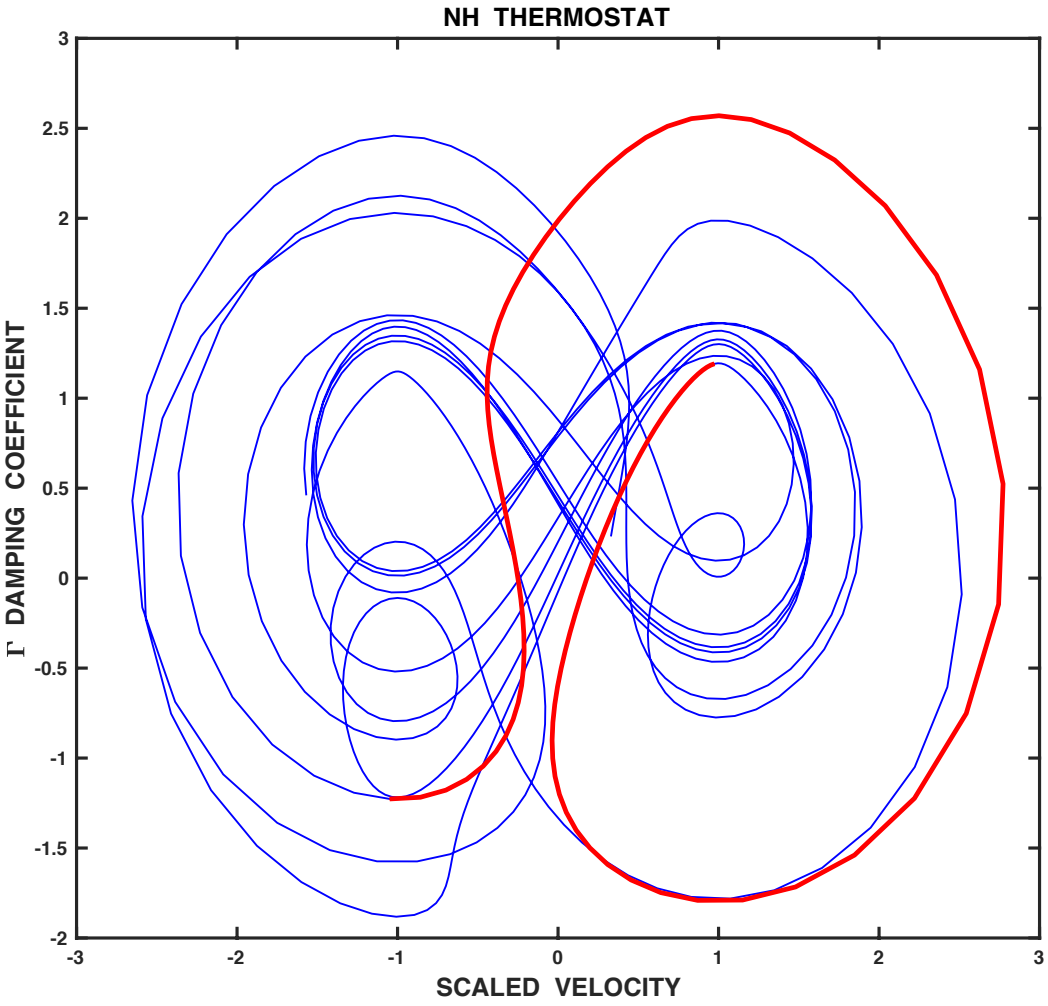

FIG. 5. (Color on line) Phase-space (Γ, u) evolution associated with Fig. 4. The blue curve corresponds to the longer-time interval shown in the top panel, Fig. 4a). The red curve is the phase-space trajectory associated with the expanded pulse in the bottom panel, Fig. 4b). The flight around the quasi-stationary point $(\Gamma = 0, u = 1)$ is the Lorentzian pulse, lasting a characteristic time $\tau_L = 0.51$.

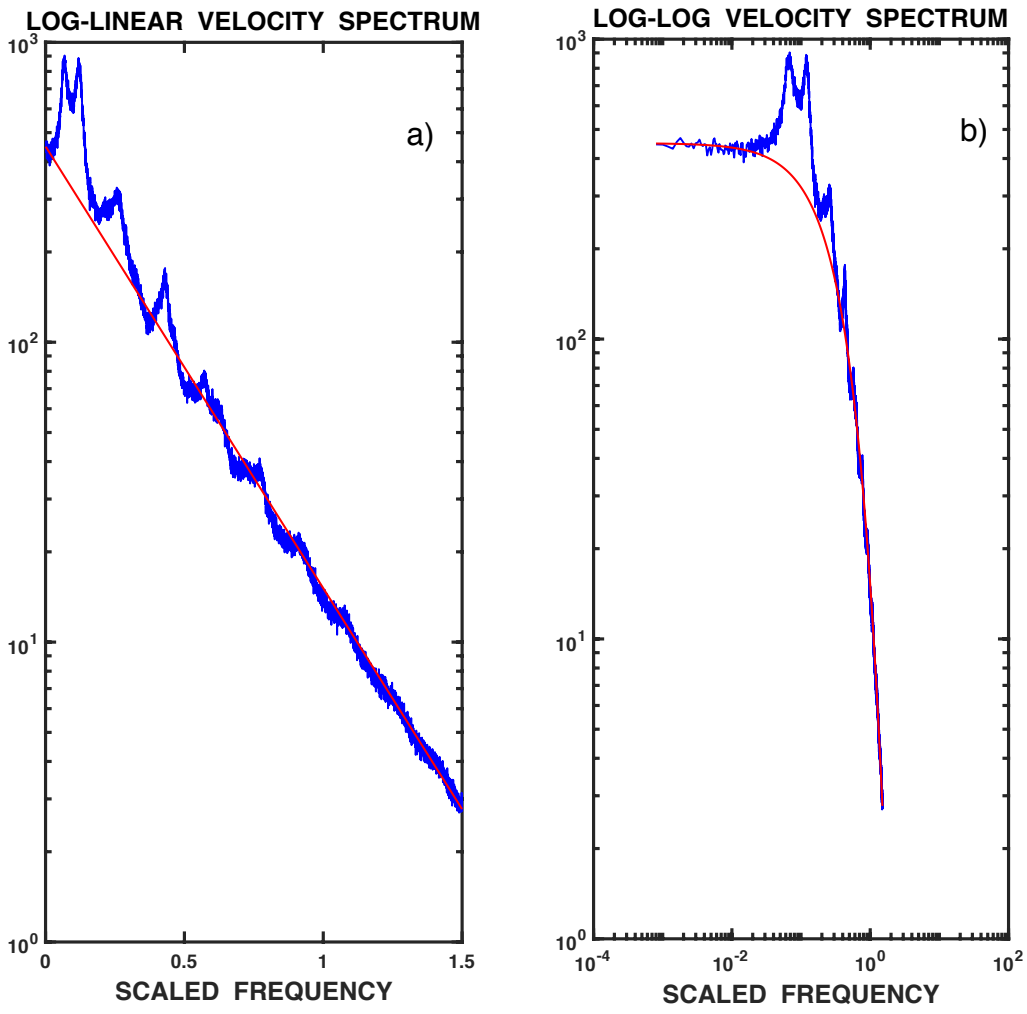

FIG. 6. (Color on line) Phase-averaged, frequency spectrum of velocity variable for the NH model. The left panel a) shows a log-linear display, and the right panel b) a log-log display. The blue curve is the numerical result, averaged over 200 initial values of θ. The red curves correspond to an exponential frequency dependence with a Lorentzian temporal width $\tau_L = 0.54$.

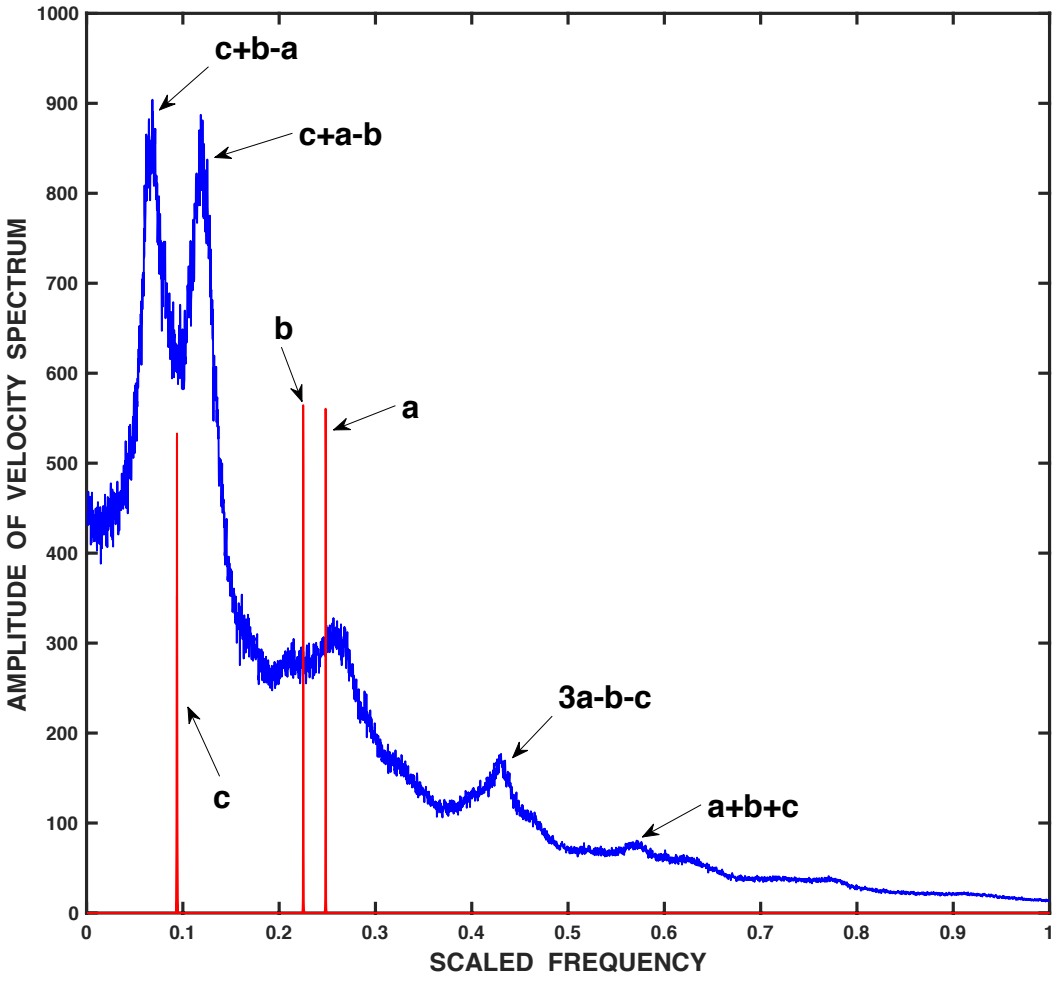

FIG. 7. (Color on line) Coherent peaks in the phase-averaged, frequency spectrum of velocity variable for the NH model. To be compared to Fig. 6. The red frequency-markers labeled (a, b, c) correspond to the intrinsic frequencies of the system: $a = 1.56$, $b = \sqrt{2}$, $c = 0.59$. The nonlinearly-generated, spectral lines are all combinations of these basic frequencies, as identified by the arrows next to them.

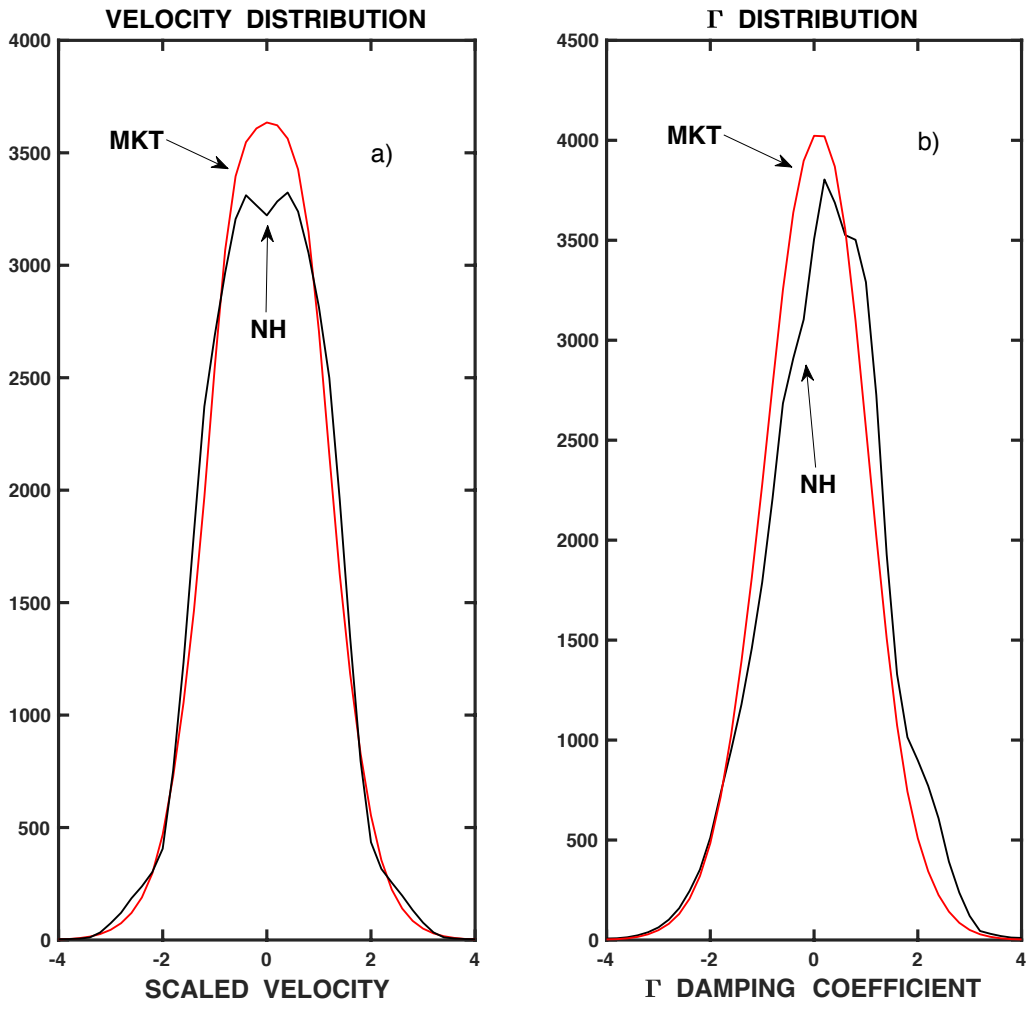

FIG. 8. (Color on line) The velocity distribution functions for the MKT and NH models are shown in the left panel a), and the corresponding distributions for the Γ damping coefficient are displayed in the right panel b), all using a linear scale. The MKT curves are smoother because they are averaged over an ensemble that is 50 times larger than for the NH system.

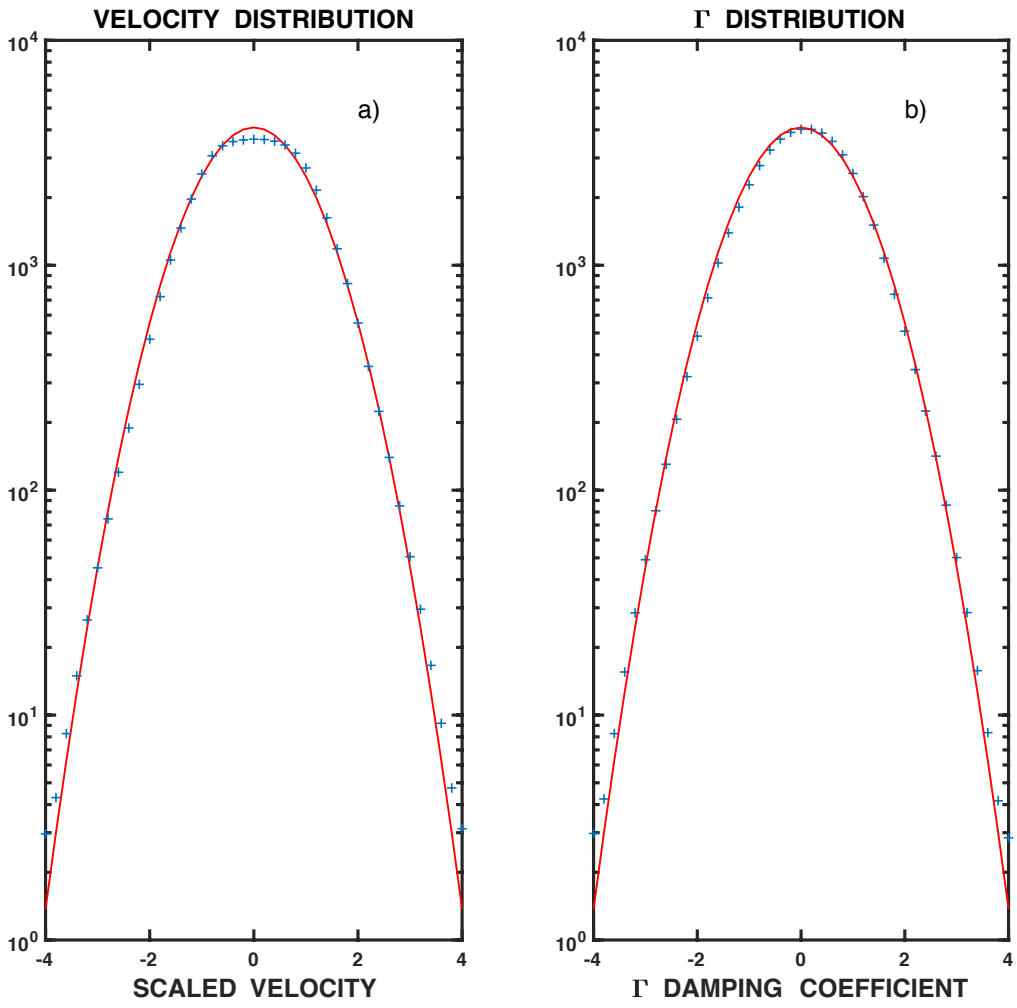

FIG. 9. (Color on line) Distribution functions for the MKT model displayed in a log-linear scale. The blue crosses are the individual values from the numerical solution and the red curve is a Maxwellian distribution with $\bar{u}^2 = 1$. Left panel a): velocity distribution function. Right panel b): distribution function of Γ damping coefficient.

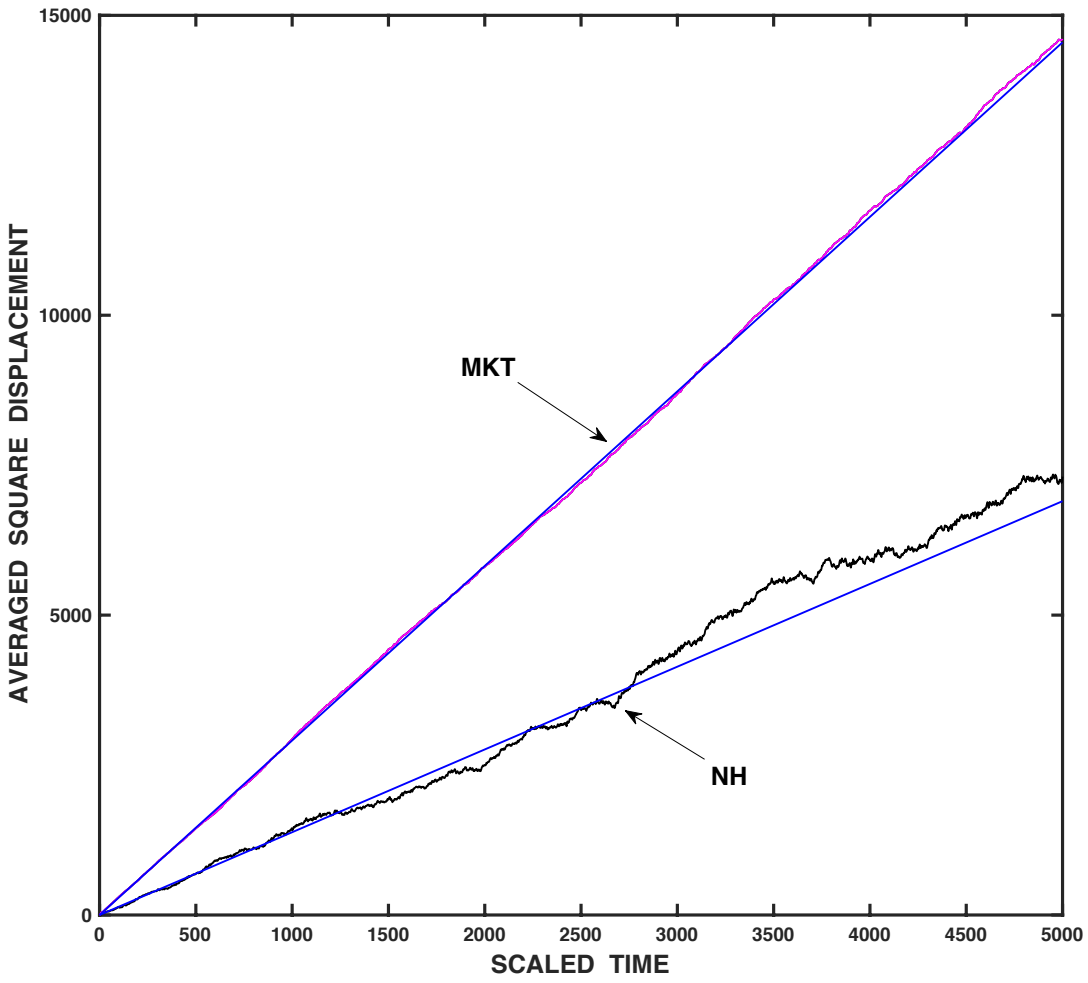

FIG. 10. (Color on line) Time evolution of the averaged, square displacement, $\langle(\triangle x/l)^2\rangle$, for the MKT and NH models demonstrates that the behavior is diffusive. The blue straight-lines are fits to the numerical solution; their slope determines the value (twice) of the respective diffusion coefficient. The MKT curve shows smaller fluctuations because it is averaged over an ensemble that is 50 times larger than for the NH system.

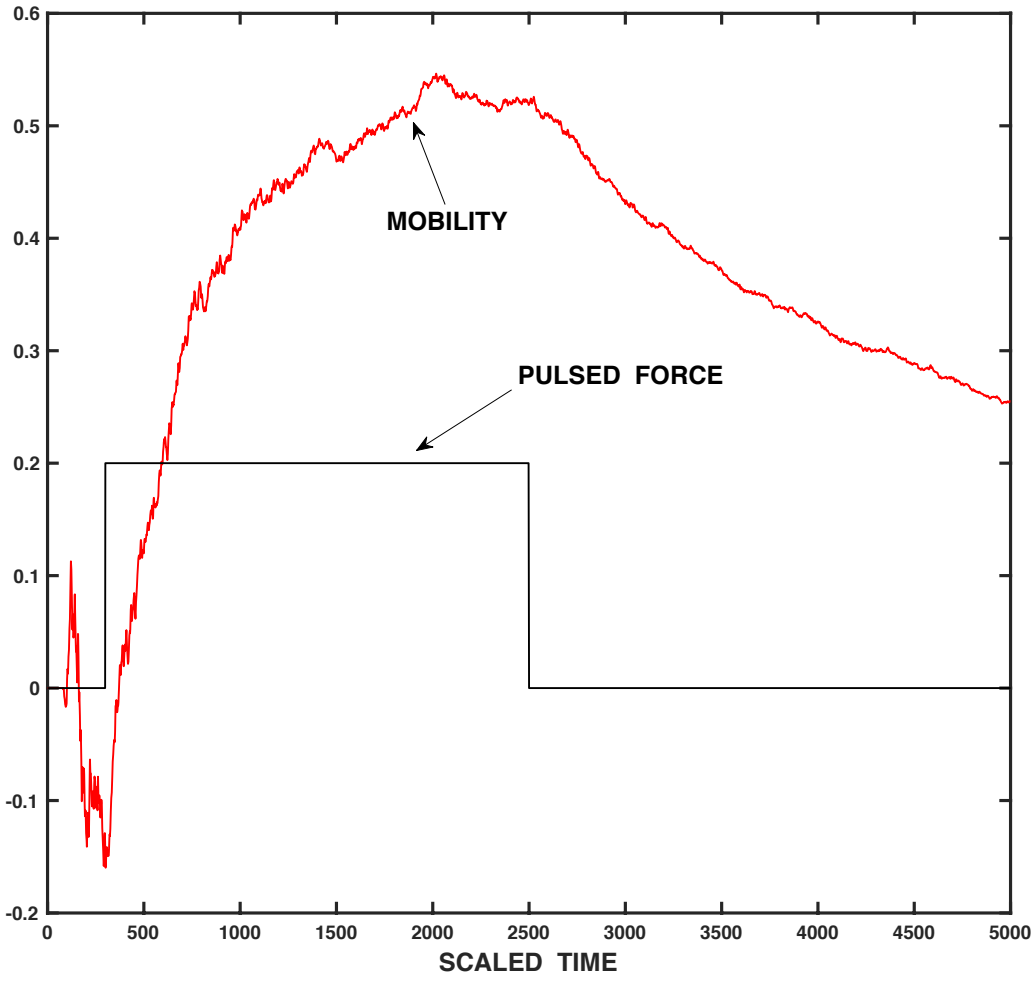

FIG. 11. (Color on line) Response to a pulsed, constant force for the NH model. Red curve is the scaled, average-velocity, $\langle u \rangle_{\tau,\theta}$, divided by the peak strength of the force, i.e., the mobility. The average is over time, and over initial phases. A steady flow is established from which the Einstein relation is tested, using the diffusion coefficient from Fig. 10. The temporal shape of the applied pulse is shown near the bottom. After the pulse is off, the mean velocity decays.

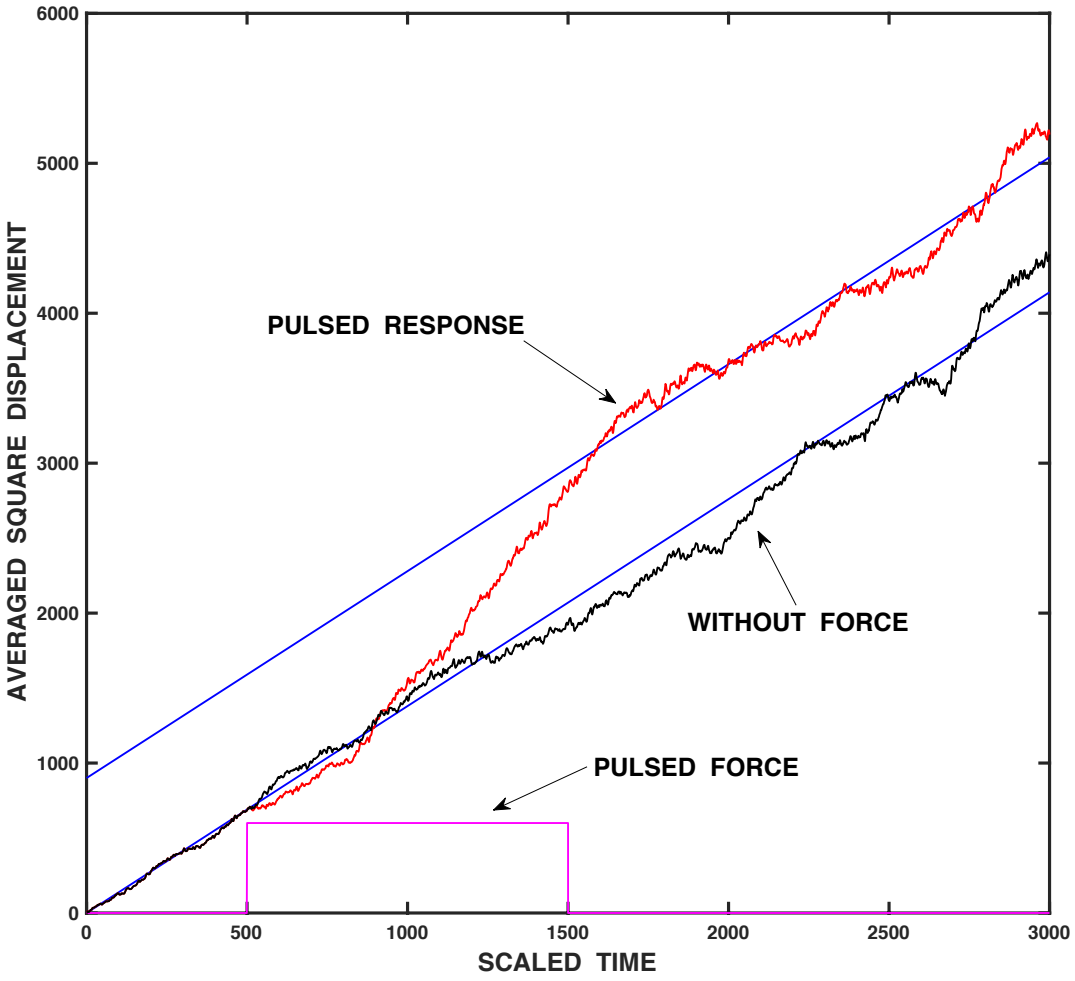

FIG. 12. (Color on line) Transition from diffusive to ballistic behavior for the NH model. The red curve is the temporal evolution of the averaged, square displacement, $\langle(\triangle x/l)^2\rangle$, resulting from the application of a pulsed-force. The black curve is the diffusive behavior without the force. The two blue, straight-lines signal path of diffusive behavior obtained from Fig. 10. They are connected by a regime of ballistic behavior (parabolic) during application of the pulse. After the pulse is off, the diffusive behavior returns.